PERGAMON

Engineering Fracture Mechanics 70 (2003) 853–870

Engineering Fracture Mechanics

www.elsevier.com/locate/engfracmech

A design approach for the mechanical properties of polypropylene discontinuous fiber reinforced cementitious composites by extrusion molding

Hiroyuki Takashima [a,*], Kiyotaka Miyagai [a], Toshiyuki Hashida [b], Victor C. Li [c]

[a] *Technical Research Laboratory, Kurabo Industries Ltd., 14-5 Shimokida-cho, Neyagawa, Osaka 572-0815, Japan*

[b] *Fracture Research Institute, Graduate School of Engineering, Tohoku University, 01 Aramaki Aza Aoba, Aoba Sendai 980-8579, Japan*

[c] *Advanced Civil Engineering Materials Research Laboratory, Department of Civil and Environmental Engineering, University of Michigan, Ann Arbor, MI 48109-2125, USA*

Abstract

Polypropylene discontinuous fiber reinforced cementitious composites were prepared by extrusion molding and tested in uniaxial tension to determine the mechanical properties such as ultimate composite strength and strain, and the critical volume fraction for multiple cracking. It was shown that the experimentally determined critical fiber volume fraction reasonably agreed with the theoretical value predicted by a micromechanics model. The extruded fiber composites yielded the ultimate composite strength of 9.0 MPa and composite strain of 0.55% at the fiber volume fraction of 7.4%. Our experimental results suggest that there is an optimal fiber aspect ratio and fiber volume fraction for enhancing the fracture properties.

Keywords: Extrusion molding; Polypropylene discontinuous fiber; Multiple cracking; Micromechanics models; Fiber orientation

1. Introduction

Extrusion molding has a potential of producing fiber reinforced cementitious composites with higher performance compared with conventional traditional molding. There are two major advantages of extrusion molding in manufacturing fiber composites: lower porosity of extruded composites due to mechanical compaction, and aligned orientation of fibers. The lower porosity may increase the composite strength and matrix toughness. In addition, the aligned fiber orientation may enhance the mechanical properties of fiber composites in the extrusion direction. One of the most effective ways for improving the ductility of cementitious composites is the use of multiple cracking phenomenon induced by fiber reinforcement. The multiple cracking phenomenon produces pseudo-strain-hardening behavior characterized by a sustained and increasing load capacity after first matrix crack [1].

* Corresponding author. Tel.: +81-72-823-8137; fax: +81-72-823-7906.
E-mail address: hiroyuki_takashima@kurabo.co.jp (H. Takashima).

0013-7944/03/$ - see front matter © 2002 Elsevier Science Ltd. All rights reserved.
PII: S0013-7944(02)00154-6

A general micromechanics model has been developed for random short fiber composites based on fracture mechanics approach [2–6]. The micromechanics model has been validated by experimental investigations on regular cast specimen [7,8]. In contrast, the design methodology for discontinuous fiber cementitious composites by extrusion molding has not yet been established. The composite parameters such as matrix and fiber parameters are being selected by a trial and error approach. There is limited research investigation on theoretical modeling of extruded discontinuous fiber reinforced cementitious composite [9–11]. Mu and Li [10] and Li et al. [11] reported their theoretical models for predicting the bend over point stress and the condition for multiple cracking for aligned short fiber reinforced composites based on an energy approach and inclusion method. They showed that the bend over point stress predicted by their model was close to the experimental value. However, the theoretical model for the condition of multiple cracking has not yet been validated experimentally.

Shah and Shao [12], Shao et al. [13] and Akkaya et al. [14] have reported that discontinuous fiber reinforced cementitious composites manufactured by extrusion showed pseudo-strain-hardening behavior. However, no attempt has been made to develop a theoretical model for the design of extruded fiber reinforced composites.

In this paper, we take advantage of the micromechanics model based on a fracture mechanics approach [2–4] to predict the mechanical properties of discontinuous fiber reinforced composite by extrusion molding, especially to predict the necessary condition for pseudo-strain-hardening behavior. We prepared extruded fiber composites using polypropylene (PP) fibers. Direct tension tests were carried out to determine the mechanical properties such as ultimate tensile stress and strain, and the critical fiber volume fraction of the extruded composites. The experimental data were compared with theoretical prediction based on the micromechanics model. The mechanical properties of the extruded composites were also compared with those of cast fiber composites in terms of interfacial friction bond strength.

2. Theory

In this paper, we adopt a simple model of fiber–matrix interface debonding based on a purely friction interface without elastic bond. The following assumptions are made to construct the micromechanics model: fibers never break; fibers are debonded and pulled out completely from the matrix; and the interfacial friction bond strength along the fiber–matrix interface is constant during the debonding and pull-out process.

Li [3] has analyzed the relationship between the fiber bridging load and displacement during fiber frictional debonding and pull-out. We adopt this relationship for aligned fiber composites. The prepeak and postpeak part of the bridging stress–displacement curve σ_B–δ can then be obtained in a normalized form (see Appendix A):

$$\tilde{\sigma}_B(\tilde{\delta}) = 2\left[2\left(\frac{\tilde{\delta}}{\tilde{\delta}^*}\right)^{1/2} - \frac{\tilde{\delta}}{\tilde{\delta}^*}\right] \quad \text{for } \tilde{\delta} \leqslant \tilde{\delta}^* \tag{1}$$

$$\tilde{\sigma}_B(\tilde{\delta}) = 2(1-\tilde{\delta})^2 \quad \text{for } 1 > \tilde{\delta} > \tilde{\delta}^* \tag{2}$$

where $\tilde{\sigma}_B \equiv \sigma_B/\sigma_0$, $\sigma_0 \equiv V_f\tau(L_f/d_f)/2$, and $\tilde{\delta} \equiv \delta/(L_f/2)$ and d_f is the fiber diameter, L_f, fiber length, τ, interfacial friction bond strength. $\tilde{\delta}^* \equiv [2\tau(1+\eta)/E_f](L_f/d_f)$ corresponds to the maximum attainable value of δ_0 normalized by $L_f/2$. The elastic modulus of the matrix and the fiber are E_m and E_f, respectively and the volume fraction of the matrix and the fiber are V_m and V_f, respectively. $\delta_0 \equiv 4l^2\tau(1+\eta)/(E_f d_f)$ corresponds to the displacement at which frictional debonding is completed for a fiber with an embedment length l and $\eta \equiv (V_f E_f/V_m E_m)$.

Marshall and Cox [15] have shown that, based on the J-integral method, the crack tip toughness J_{tip} during steady state cracking can be expressed by:

$$J_{tip} = \sigma_a \delta_a - \int_0^{\delta_a} \sigma_B(\delta)\,d\delta \tag{3}$$

where σ_a is the steady state cracking stress and δ_a is the displacement corresponding to σ_a.

Li [16] reviewed the necessary conditions of fiber volume fraction for pseudo-strain-hardening behavior. For pseudo-strain hardening with multiple cracking,

$$\sigma_a \leqslant \sigma_{pc} \tag{4}$$

$$J_{tip} \leqslant \sigma_{pc}\delta^* - \int_0^{\delta^*} \sigma_B(\delta)\,d\delta \tag{5}$$

where σ_{pc} is the the maximum value of the bridging stress–displacement curve.

Using Eqs. (1) and (2) in Eq. (5), the critical fiber volume fraction $V_{f,crit}$ for multiple cracking is given by:

$$V_f \geqslant V_{f,crit} = \frac{6d_f^2 E_f}{\tau^2 L_f^3 (1+\eta)} J_{tip} \tag{6}$$

3. Experimental procedure

3.1. Materials

The mix proportion of the matrix is shown in Table 1. All of the mix proportions are by weight of the ingredients. Discontinuous PP fibers of different length and diameter were tested in this study. The fiber dimensions and properties are shown in Table 2. The fiber volume fractions employed were in the range of 0–8.4%. The maximum achievable fiber volume fraction was 7.0%, 8.4%, and 7.5% for $L_f/d_f = 233$, 333, and 556, respectively. Further incorporation of higher fiber volume fraction was difficult because of very poor workability.

Table 1
Matrix mix proportion (by weight)

Ordinary Portland cement	Silica powder	Pulp	Mineral fiber	Methyl cellulose	Water
1.00	0.64	0.05	0.05	0.06	0.77

Table 2
Dimensions and properties of PP fibers used

Fiber type	Length, L_f (mm)	Diameter, d_f (μm)	Aspect ratio, L_f/d_f	Density (kg/m^3)	Young's modulus, E_f (GPa)	Tensile strength, σ_f (MPa)
A	10	18	556	0.91	3.70	295
B	6	18	333	0.91	3.70	295
C	10	43	233	0.91	3.70	295

3.2. Specimen preparation

In this paper, the mechanical properties of fiber reinforced composites manufactured by extrusion were compared with cast fiber composites. These composites were made of the same proportion of raw materials. The preparation for these composites is presented below.

Firstly, the raw materials were mixed for 3 min without water by an Erich mixer. Water was added into the mixture and mixed for 2 min. Cast fiber composites were prepared by the mixture using a polyethylene mold. All the specimens were machined into a rectangular coupon of size 230 mm × 40 mm × 15 mm.

Next, the mixture is kneaded for 3 min by a kneader with two blades. The kneaded mixture was used to prepare the extruded fiber composites. The extrusion molding was conducted using a ram extruder. The extruded samples had the cross section of 80 mm × 15 mm. The extruded specimens were cut into a length of 250 mm perpendicular to the extrusion direction.

The specimens of the extruded and cast composites are steam-cured for 5 h at 70 °C.

3.3. Testing procedure

The tensile behavior of the composites was determined by conducting uniaxial tension tests as shown in Fig. 1. The coupon specimens were tested under displacement control in a 50 kN material testing system. The displacement rate used was 0.5 mm/min. For gripping purpose, aluminum plates were glued by epoxy resin onto the ends of the tension specimens. A linear variable differential transducer was used to measure the displacement between two points on the specimen at a gage length of 50 mm.

Three point bending tests were conducted to determine the fracture toughness of the matrix K_m, following ANSI/ASTM E 399 (standard test method for plane-strain fracture toughness of metallic materials). The dimensions of the three point bending specimens are shown in Fig. 2. A prenotch was introduced by a diamond wheel saw, and the tip of the prenotch was sharpened with a silicon carbide blade. The notch tip

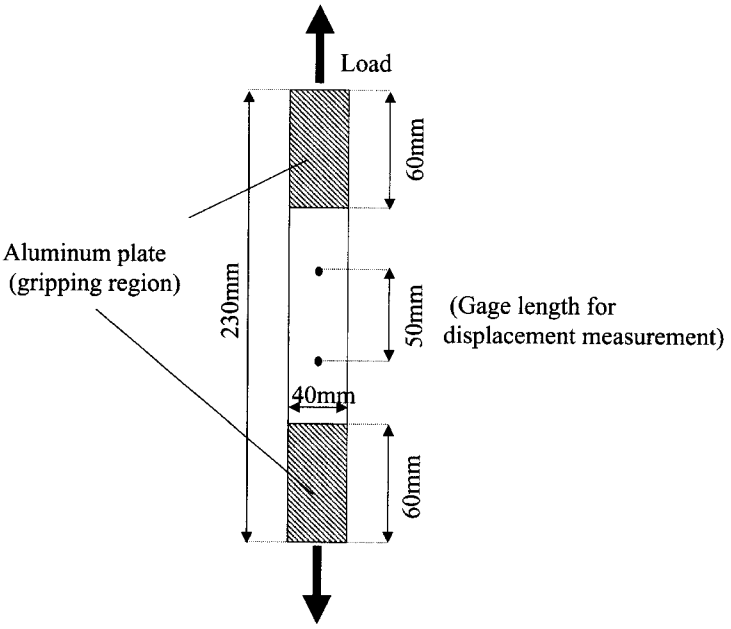

Fig. 1. Specimen configuration of tension test.

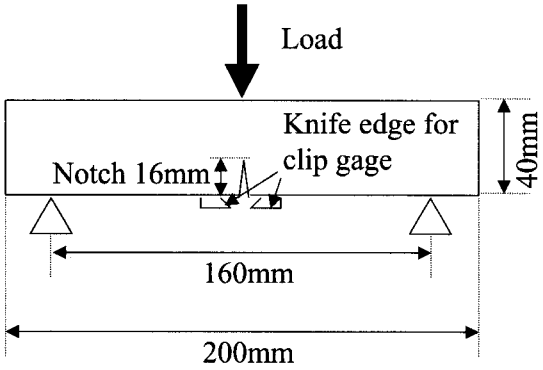

Fig. 2. Specimen configuration of fracture toughness test.

radius was approximately 0.15 mm. The specimens were loaded until a fast fracture took place. The crack opening displacement was monitored by a displacement transducer (clip gage) in addition to the applied load. Three specimens were tested for the same fiber volume fraction and the results were averaged. The experimental data presented in the following sections are averaged data.

3.4. Fiber orientation and fiber volume fraction

The cross section perpendicular to the extrusion direction was observed by scanning electron microscopy (SEM) using both extruded and cast composites in order to examine the fiber orientation. As shown in Fig. 3, it is possible to determine the distribution of fiber orientation based on the fiber shape of cross section perpendicular to the extrusion direction, because the PP fibers have an exact circular cross section. The orientation of each fiber axis, with respect to the plane perpendicular to the extrusion direction, θ is estimated by approximating the fiber cross section as an elliptical shape, and is given by the following equation:

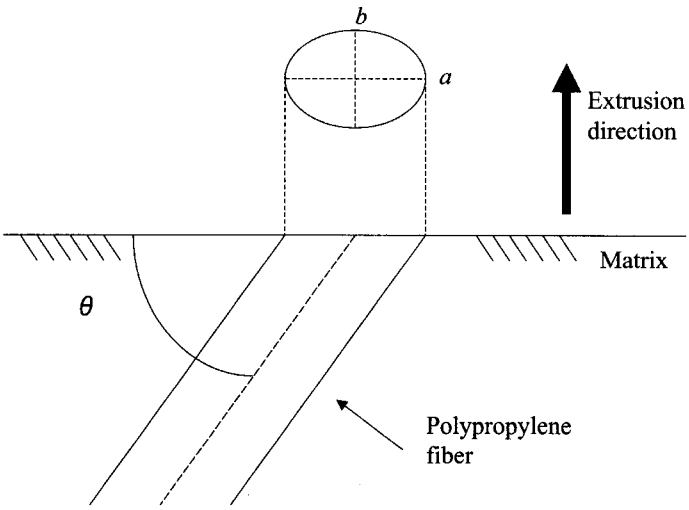

Fig. 3. Fiber orientation.

$$\theta = \sin^{-1}\left(\frac{b}{a}\right) \tag{7}$$

where a and b are the major and minor axis, respectively. Aligned fibers with respect to the extrusion direction correspond to 90°.

The fiber volume fraction was also determined based on the SEM observation of the cross section perpendicular to the extrusion direction. The ratio of the total area of fibers on the cross section to the inspection area of the SEM observation was computed to obtain the fiber volume fraction. Hereafter, the fiber volume fraction determined using cross sections is referred to as $V_{f,real}$. The use of $V_{f,real}$ and Eq. (6) implies that mechanical interactions before inclined fiber and matrix at exit point, such as the snubbing phenomenon discussed in Li et al. [2], are not taken into account in the present analysis.

4. Results and discussion

4.1. Fiber orientation

Fiber orientation is one of the most important factors influencing the mechanical properties of fiber reinforced composites. Fig. 4(a) and (b) shows an example of SEM observations of fiber dispersion for the extruded and cast composite, respectively. The PP fibers are observed as dark spots in the photographs.

The distribution of fiber orientation was determined from the SEM observations of cross sections perpendicular to the extrusion direction as described in Section 3. The distribution of fiber orientation obtained for the extruded and cast composites is shown in Fig. 5. L_f/d_f of PP fiber is 333 and the volume fraction $V_{f,real}$ of the extruded composite is 3.1% and 3.3% for the cast composite. It is noted in the extruded composites that approximately 80% of the fibers are aligned with respect to the extrusion direction for $L_f/d_f = 333$. In the cast composites a broad distribution is seen in the range of 9–63°.

The ratio of the aligned fibers is plotted in Fig. 6 for the extruded composites as a function of $V_{f,real}$. It can be noted that no drastic variation in the aligned fiber ratio is observed irrespective of the different $V_{f,real}$, although the ratio appears to decrease slightly with increasing $V_{f,real}$ for the large fiber aspect ratio, $L_f/d_f = 556$. It is expected that the larger the fiber aspect ratio, the greater the aligned fiber ratio. Indeed, the aligned fiber ratio for $L_f/d_f = 333$ is larger than that for $L_f/d_f = 233$. It is observed, however, that the fiber aspect ratio of 556 gives a significantly lower aligned fiber ratio. In the extruded composites of $L_f/d_f = 556$, fiber clustering has been shown to occur during the mixing process. The interaction between individual fibers may reduce the number of aligned fibers in the extrusion process. This may explain the lower aligned fiber ratio for $L_f/d_f = 556$. It can be understood that the fiber aspect ratio significantly affects the fiber distribution in extruded composites.

The aligned fibers in the extruded composites are expected to have a greater influence on the mechanical properties relative to the inclined fibers. In this study, the effective fiber volume fraction $V_{f,eff}$ was calculated by multiplying $V_{f,real}$ by the aligned fiber ratio for each extruded composites and used to estimate the composite mechanical properties based on the micromechanics model.

4.2. Interfacial friction bond strength

The frictional bond strength at the PP fiber/matrix interface was determined from the uniaxial tension tests, and the mechanical properties of the extruded and cast composites are compared in terms of the interfacial friction bond strength. The fiber pull-out behavior and load–displacement behavior in the fiber composites is presented first. Microphotographs of the fiber pull-out behavior are given in Fig. 7 for the extruded composites. Complete fiber pull-out is observed for $L_f/d_f = 233$ and 333, whilst fiber break takes

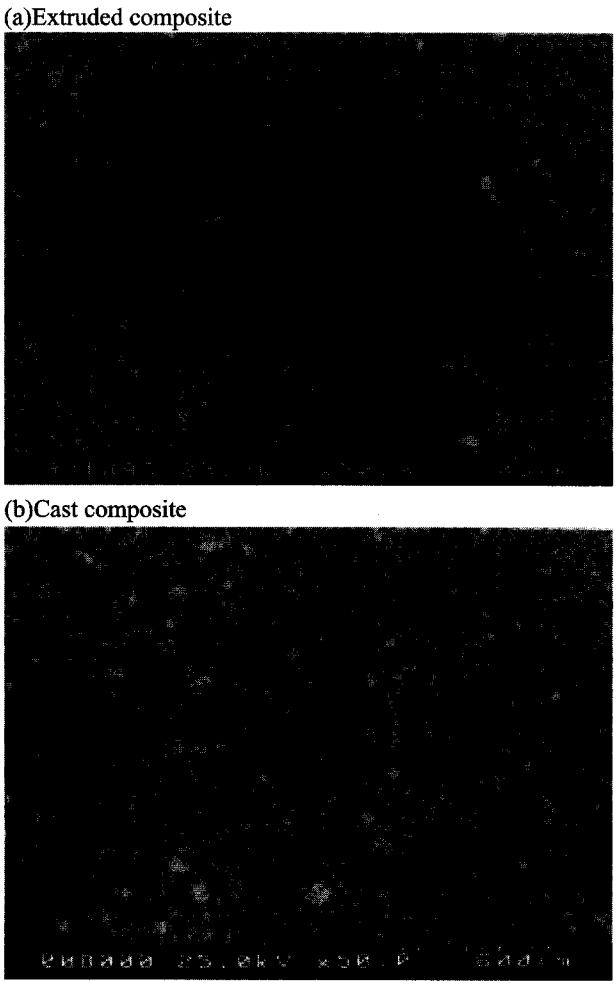

Fig. 4. Comparison of microstructures of extruded (a) and cast (b) composites; $L_f/d_f = 333$. Black spots and ellipses represent fibers.

place for $L_f/d_f = 556$ with the maximum pull-out length being less than half of the initial fiber length. This observation can be supported from load–displacement records. The load–displacement curves of the uniaxial tension specimens are shown in Fig. 8 for the extruded composites. As shown in the insert, the postpeak part of the load–displacement curves can be used to estimate the fiber pull-out length. The estimated fiber pull-out length is 4.66, 2.67, and 0.92, for $L_f/d_f = 233$, 333, and 556, respectively. The estimated fiber pull-out length is close to half of the initial fiber length for $L_f/d_f = 233$ and 333, whereas the estimated value is significantly smaller compared with the half length for $L_f/d_f = 556$. The comparison confirms the above observation of the fiber pull-out behavior. Complete fiber pull-out has also been observed for the cast composites.

Fig. 9 shows tensile stress versus strain curves of PP fiber reinforced composites of $V_{f,real} = 0\%$, 1.0% and 4.5% prepared by extrusion molding. L_f/d_f is 333. The fracture behavior of the matrix ($V_{f,real} = 0\%$) and the composite of $V_{f,real} = 1.0\%$ is characterized by the formation of a single crack, even though the 1% fiber composite shows a gradual stress decrease due to the fiber bridging action. On the other hand, the fiber composite of $V_{f,real} = 4.5\%$ indicates pseudo-strain-hardening behavior due to matrix multiple cracking. The

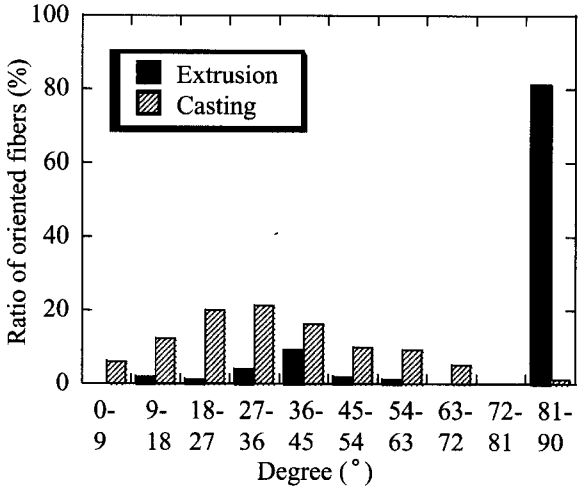

Fig. 5. Distributions of fiber orientation of extruded and cast composites; $L_f/d_f = 333$.

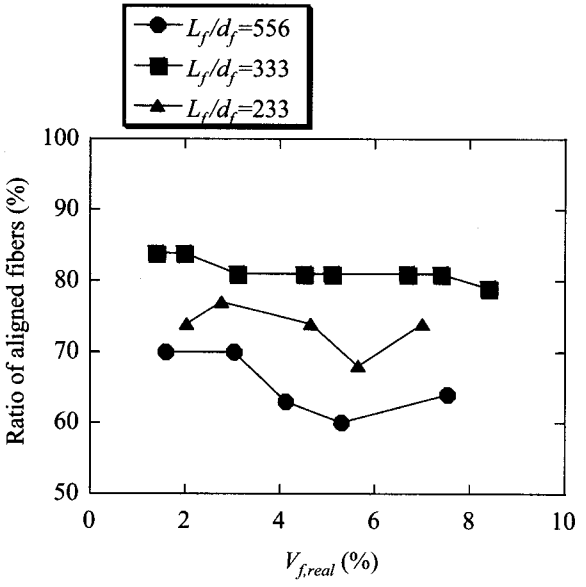

Fig. 6. Ratio of aligned fibers.

first cracking strength of $V_{f,real} = 4.5\%$ is about 25% higher than that of the matrix only. In particular, the composite strain at peak stress significantly increases by 1140% compared with that of the matrix.

In principle, the interfacial friction bond strength should be determined by conducting a single fiber pull-out test [17–19]. In this study, an estimate of the interfacial friction bond strength τ was obtained from the uniaxial tension tests indirectly.

As detailed in Appendix A, the fracture energy due to fiber pull-out in aligned fiber composites is expressed by:

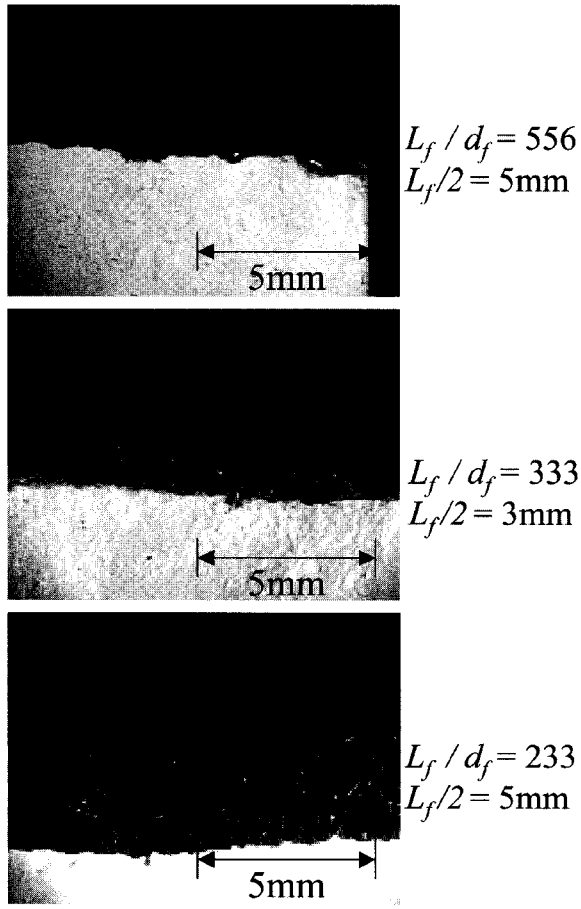

Fig. 7. Fiber pull-out and break.

$$G_b = \frac{1}{6}\tau V_f d_f \left(\frac{L_f}{d_f}\right)^2 \tag{8}$$

If the fracture energy G_b is determined for an aligned fiber composite, the interfacial friction bond strength can then be estimated from the fiber volume fraction and dimensions using Eq. (8). G_b may be obtained experimentally based on uniaxial tension tests using the following equation:

$$G_b = \frac{A}{wt} \tag{9}$$

where w is the width of the specimen and t is the thickness of the specimen. As shown in Fig. 10, the area under the load–displacement curve after the peak load is used to determine the area A.

Using Eqs. (8) and (9), τ was determined for extruded fiber reinforced composites. For random short fiber reinforced composites, Li demonstrated the fracture energy due to fiber pull-out [4]:

$$G_b = \frac{1}{12} g \tau V_f d_f \left(\frac{L_f}{d_f}\right)^2 \tag{10}$$

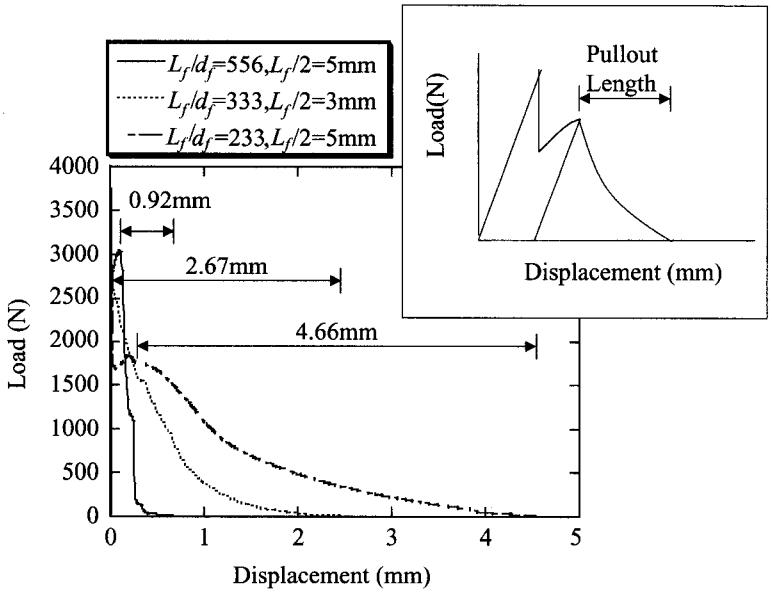

Fig. 8. Load–displacement curves.

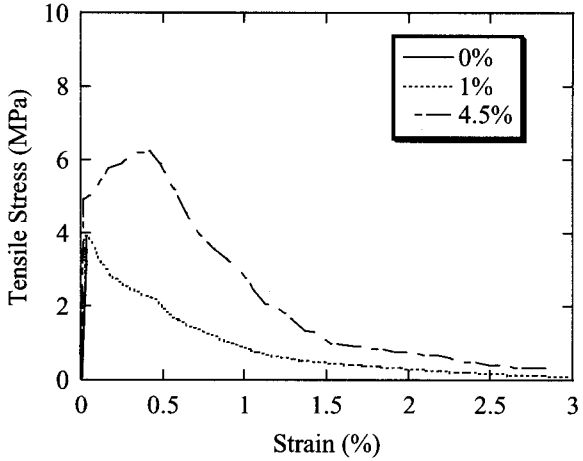

Fig. 9. Tensile stress–strain curves of the extruded composites; $L_f/d_f = 333$.

where g is the snubbing factor. τ was computed for the cast composites using Eq. (10). The value of g was assumed to be 1.6 following Refs. [3,4]. Comparison between Eqs. (8) and (10) suggests that the loss of fibers due to random orientation is approximately compensated by the inclined fiber snubbing effect. This justifies our adoption of the aligned fiber composite model and ignoring the snubbing effect for analyzing the experimental data.

Fig. 11 shows the dependence of the interfacial friction bond strength τ (normalized by initial bond strength τ_i) on the effective fiber volume fraction $V_{f,eff}$. Using Eq. (8), initial bond strength was determined for the composites of $V_{f,eff} < 1.5\%$. τ_i was 0.32 and 0.24 MPa, for $L_f/d_f = 233$ and 333, respectively. τ_i of the

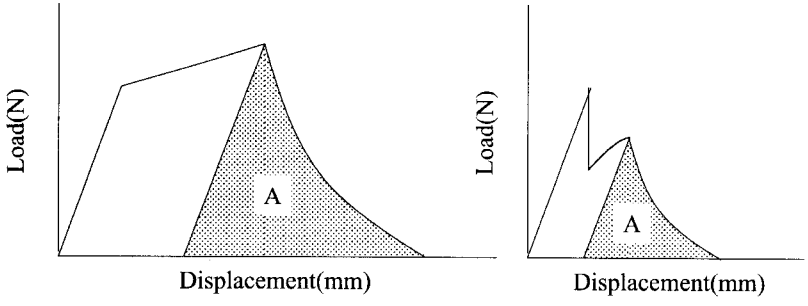

Fig. 10. Load–displacement curve.

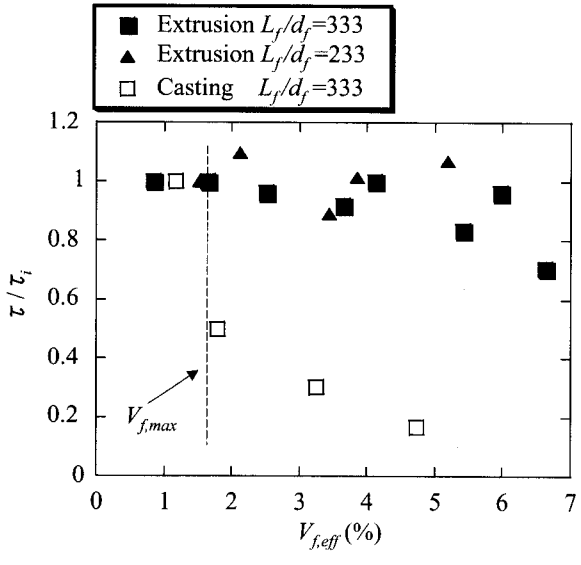

Fig. 11. Dependence of τ/τ_i on $V_{f,eff}$.

cast composite was 0.30 MPa calculated by Eq. (10). No attempt to determine the interfacial friction bond strength was made for $L_f/d_f = 556$, because fiber breakage occurred in the composite. In the extruded composites, τ is found to be approximately constant within the range of the fiber volume fractions used in this study. For the cast composites, however, τ decreases rapidly with increasing fiber volume fraction.

Milewski [20] and Evans and Gibson [21] expressed the maximum packing volume fraction $V_{f,max}$ for rod-like reinforcement:

$$V_{f,max} = \frac{5.3}{L_f/d_f} \tag{11}$$

The maximum packing volume fraction is defined as the point at which the randomly oriented fibers have no longer any rotational freedom due to the restrictions of neighboring fibers.

It is expected that for a fiber volume fraction greater than $V_{f,max}$, the distributed fibers will start to touch each other, causing a reduction in interfacial friction bond strength. The packing volume fraction appears to provide a measure of appropriate volume fraction for producing uniform fiber composites. According to

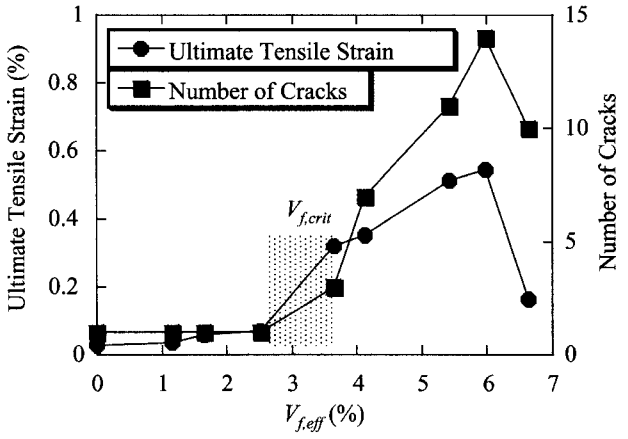

Fig. 12. Dependence of number of cracks and ultimate tensile strain on $V_{f,eff}$, $L_f/d_f = 333$. The critical fiber volume fraction $V_{f,crit}$ exists in shaded area.

Eq. (11), the value of $V_{f,max}$ is equal to 1.6% for the L_f/d_f of 333 used in this study. As shown in Fig. 11, τ of the cast composite decreased when $V_{f,eff}$ exceeded $V_{f,max}$.

This comparison suggests that extrusion molding allows us to incorporate a larger volume of fiber compared to conventional casting, without loss of fiber/matrix bond efficiency.

4.3. Critical fiber volume fraction

Fig. 12 shows the number of multiple cracks which occurred on the specimens and ultimate tensile strain as a function of $V_{f,eff}$ for the extruded composites. L_f/d_f of PP fiber is 333. For the composites of $V_{f,eff} < 2.5\%$, only a single crack was observed. Multiple cracking phenomenon took place for $V_{f,eff} > 3.6\%$. The critical fiber volume fraction for multiple cracking $V_{f,crit}$ is judged to be in the range of 2.5–3.6%, as indicated by the shaded area in Fig. 12.

Theoretically the critical fiber volume fraction for multiple cracking can be obtained from Eq. (6). The fiber parameters are shown in Table 2. The interfacial friction bond strength is assumed to be 0.24 MPa based on calculations of inverting measured G_b for τ as described in the previous section. The crack tip toughness J_{tip} in Eq. (6) may be approximated as:

$$J_{tip} \approx \frac{K_m^2}{E_m} \tag{12}$$

where K_m and E_m are the matrix fracture toughness and Young's modulus. The matrix fracture toughness was computed from the peak load measured by the three point bending tests. The average K_m value is 1.07 MPa $m^{1/2}$. The simple compliance method was employed to determine the matrix Young's modulus using the initial slope of the load–crack opening displacement curves determined by the three point bending tests, following ANSI/ASTM E399. The compliance method showed that the average value of E_m is 21.4 GPa.

Eq. (6) yields the value of 3.1% for the critical fiber volume fraction for the composite containing fibers with $L_f/d_f = 333$. It is shown that the critical fiber volume fraction predicted by the micromechanics model reasonably agrees with the experimental results.

As shown in Fig. 13, the ultimate tensile strain is plotted for the extruded composites of $L_f/d_f = 233$ and 556. Multiple cracking behavior is seen to take place in the range of $V_{f,eff} = 3.9$–5.2% and 2.1–2.6% for composites of $L_f/d_f = 233$ and 556, respectively, even though the strain increase is less significant compared

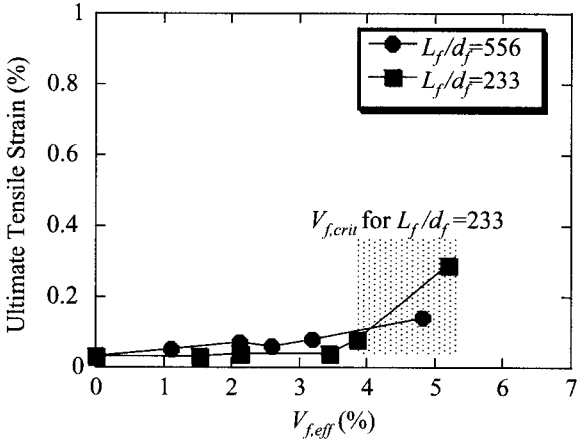

Fig. 13. Dependence of ultimate tensile strain on $V_{f,eff}$.

to the composites of $L_f/d_f = 333$. The limited strain enhancement for $L_f/d_f = 556$ may be due to the extensive fiber breakage in the composites. For the composites of $L_f/d_f = 233$, the introduction of larger fiber volume fractions was impractical due to extremely poor workability. Thus, the maximum achievable V_f was 7.0% for $L_f/d_f = 233$, which corresponds to $V_{f,eff} = 5.2\%$. Even though the data for the higher volume fractions are limited, it can be seen that the model predicted $V_{f,crit}(= 3.8\%)$ is consistent with the experimental result, again supporting the validity of the micromechanical model.

As described above, τ is estimated from the fracture energy of the composite based on the micromechanical model derived for the aligned fiber case. The computed τ is 0.32 and 0.24 MPa, for $L_f/d_f = 233$ and 333, respectively. The slightly greater value of τ in the composite of $L_f/d_f = 233$ may be due to the fact that the composite has the lower ratio of aligned fibers than that for $L_f/d_f = 333$. The model for predicting $V_{f,crit}$ is also developed for aligned fiber composites. Thus, the τ value estimated from the fracture energy of each composite was used to predict $V_{f,crit}$. Further study is required to take into account the contribution from inclined fibers with respect to the matrix crack in order to develop a more accurate model for determining τ and predicting $V_{f,crit}$.

4.4. Tensile fracture properties

Fig. 14 shows the ultimate tensile stress for the extruded and cast composites as a function of $V_{f,eff}$. The ultimate tensile stress of the cast composite showed a relatively constant value regardless of the fiber addition and gradually decreased for the fiber volume fraction $> V_{f,max}$, reflecting the reduction in the interfacial friction bond strength. The extruded matrix specimen gave higher tensile strength than that of the cast matrix, due to the increased density for the extruded matrix (1400 kg/m^3) relative to 1200 kg/m^3 for the cast matrix.

In the extruded composites, the ultimate tensile stress steadily increased with increasing fiber volume fraction. The ultimate tensile stress for $L_f/d_f = 333$ and 556 gives a higher value than that for $L_f/d_f = 233$. However, the ultimate tensile stress of $L_f/d_f = 556$ is close to that for $L_f/d_f = 333$ due to the fiber break, regardless of the larger fiber aspect ratio. For $L_f/d_f = 333$ and 556, the ultimate tensile stress reaches approximately 9.0 MPa at $V_{f,eff} = 6\%$ ($V_{f,real} = 7.4\%$). This ultimate tensile stress of 9.0 MPa is one of the highest values obtained for extruded discontinuous fiber reinforced cementitious composites. The ultimate tensile stress and strain capacity are summarized in Fig. 15 for the extruded and cast composites. It can be noted that the fiber aspect ratio of 333 is an optimal condition for the fracture properties.

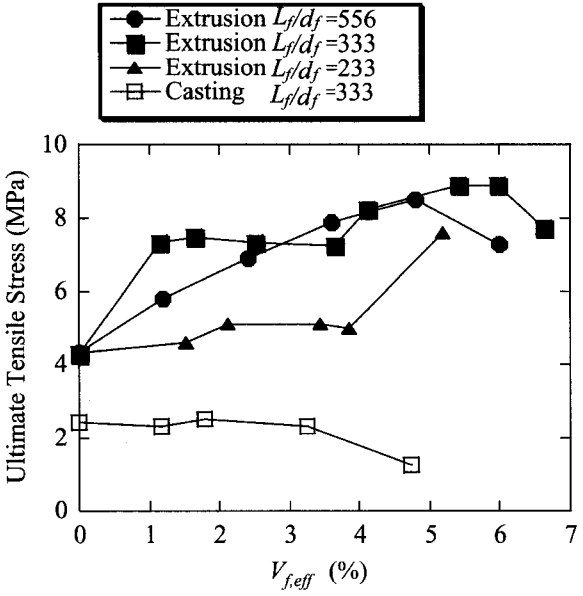

Fig. 14. Dependence of ultimate tensile stress of the extruded and cast composites on $V_{f,eff}$.

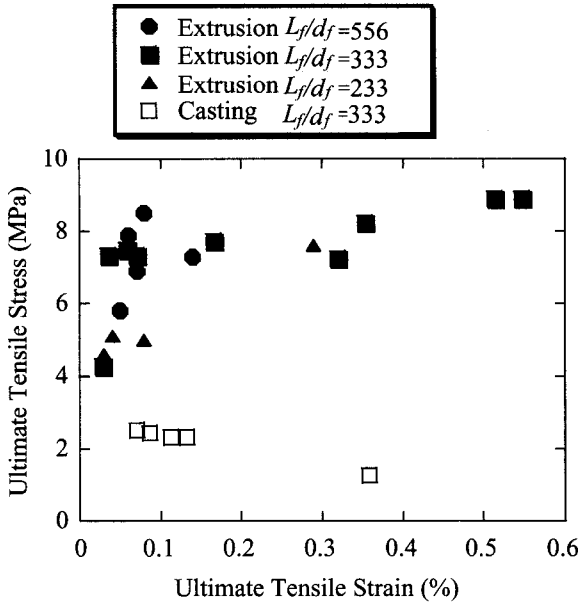

Fig. 15. The ultimate tensile stress and strain capacity of the extruded and cast composites.

Shah and coworkers reported mechanical properties of extruded composites using several kinds of fibers [13,14,22]. Fig. 16 shows a comparison of the data of Shah and coworkers and our experimental results obtained in this study for extruded PP and polyvinyl alcohol (PVA) discontinuous fiber composites. No

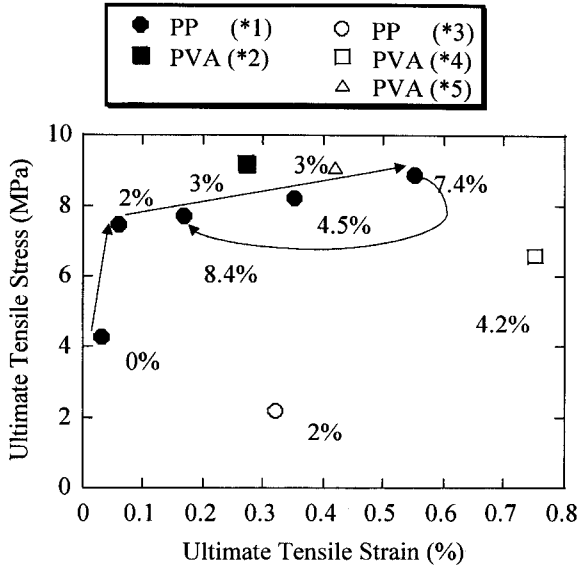

Fig. 16. Comparison of the data in this paper and other researchers; (*1) this paper, (*2) Takashima et al. [23], (*3) Shao et al. [13], (*4) Shao and Shah [22], (*5) Akkaya et al. [14].

detailed information of the fiber distribution has been reported in the literature [13,14,22]. Thus, the data of $V_{f,real}$ indicated in Fig. 16 for comparison purpose. Our data for PVA fiber composite is as follows: $d_f = 0.040$ mm, $L_f = 6$ mm, $\sigma_f = 1600$ MPa, and $E_f = 40$ GPa [23]. Except for the matrix and the composite of $V_{f,real} = 2\%$ tested in this study, all of the composites have shown pseudo-strain hardening.

It should be mentioned here that excessive addition of discontinuous fibers cause a decrease of the ultimate tensile stress and strain, as illustrated in Figs. 14 and 16. The largest volume fraction of $V_{f,real} = 8.4\%$ results in ultimate tensile stress which is slightly decreased. This observation may suggest that there is an optimal fiber volume fraction for the mechanical properties of extruded discontinuous fiber reinforced composites. As shown in Fig. 16, our composites with higher tensile stress show a smaller strain capacity compared with the composites prepared by Shah and coworkers In addition, the density of the composites is significantly smaller than that of Shah and coworkers.

Wu and Li [24] have shown that it becomes more difficult to induce multiple cracking in the case of high matrix toughness. This is the case for our fiber composites. Further improvement in the mechanical properties, particularly for enhancement in strain capacity of such high matrix toughness composites, calls for tailoring the interfacial and/or fiber properties.

5. Conclusions

In this paper, we present a design approach on the basis of a micromechanics model for the mechanical properties of aligned fiber reinforced composite, especially the critical fiber volume fraction for pseudo-strain hardening. In order to support the micromechanics model, uniaxial tension tests were conducted on PP discontinuous fiber reinforced cementitious composites manufactured by extrusion molding. The critical fiber volume fraction was determined experimentally from ultimate tensile strain and number of multiple cracks versus fiber volume fraction relationship.

The theoretical critical fiber volume fraction predicted by the micromechanics model for the extruded composite was found to reasonably agree with the experimental data, thus validating the micromechanical model.

For comparison, cast fiber reinforced composites were tested in addition to the extruded composites. A comparison of the extruded and cast fiber composites indicated that the extrusion molding allows us to incorporate a larger volume of fibers and to improve the mechanical properties of fiber composites compared to conventional casting. The highest ultimate tensile stress of our extruded fiber composite reached 9.0 MPa and the strain capacity was up to 0.55%.

Appendix A

A.1. Single fiber stress–displacement curve for aligned fiber reinforced composite

Consider a single fiber with a diameter d_f, length L_f, an interfacial friction bond strength τ and a snubbing coefficient f. The elastic modulus of matrix and fiber are E_m and E_f, respectively and the volume fraction matrix and fiber are V_m and V_f, respectively.

Li et al. [2] showed that the bridging stress–displacement curve can be predicted by integrating the contribution of individual fibers crossing a matrix crack plane:

$$\sigma_B(\delta) = \frac{4V_f}{\pi d_f^2} \int_{\varphi=0}^{\pi/2} \int_{z=0}^{L_f/2\cos\varphi} P(\delta)p(\varphi)p(z)\,dz\,d\varphi \tag{A.1}$$

where $P(\delta)$ is the fiber bridging load versus displacement δ, $p(\varphi)$ and $p(z)$ are the probability-density functions of the orientation angle and centroidal distance of fibers from crack plane.

Li [3] has shown that during frictional debonding, the fiber bridging load versus displacement can be obtained from a shear–lag analysis:

$$P(\delta) = \frac{\pi}{2}\sqrt{(1+\eta)E_f d_f^3 \tau \delta}\, e^{f\varphi} \quad \text{for } \delta \leqslant \delta_0 \tag{A.2}$$

where $\delta_0 \equiv 4l^2\tau(1+\eta)/(E_f d_f)$ corresponds to the displacement at which frictional debonding is completed for a fiber with embedment length l and $\eta \equiv (V_f E_f / V_m E_m)$.

After the fiber is fully debonded, a fiber pull-out load versus displacement curve can be given by the following equation [3]:

$$P(\delta) = \pi\tau l d_f \left(1 - \frac{\delta}{l}\right) e^{f\varphi} \quad \text{for } \frac{l}{2} \geqslant \delta \geqslant \delta_0 \tag{A.3}$$

For uniformly aligned fiber distribution ($\varphi = 0$), $p(\varphi) = 1$ and $p(z) = 2/L_f$ [2]. Using Eqs. (A.2) and (A.3) in Eq. (A.1), the prepeak part of the bridging stress–displacement curve can be obtained in normalized form:

$$\tilde{\sigma}_B(\tilde{\delta}) = 2\left[2\left(\frac{\tilde{\delta}}{\tilde{\delta}^*}\right)^{1/2} - \frac{\tilde{\delta}}{\tilde{\delta}^*}\right] \quad \text{for } \tilde{\delta} \leqslant \tilde{\delta}^* \tag{A.4}$$

where $\tilde{\sigma}_B \equiv \sigma_B/\sigma_0$, $\sigma_0 \equiv V_f\tau(L_f/d_f)/2$, and $\tilde{\delta} \equiv \delta/(L_f/2)$. $\tilde{\delta}^* \equiv [2\tau(1+\eta)/E_f](L_f/d_f)$ corresponds to the maximum attainable value of δ_0 normalized by $L_f/2$ for the fiber with the longest embedment length of $L_f/2$.

The postpeak part of the bridging stress–displacement curve can be obtained in normalized form:

$$\tilde{\sigma}_B(\tilde{\delta}) = 2(1-\tilde{\delta})^2 \quad \text{for } 1 > \tilde{\delta} > \tilde{\delta}^* \tag{A.5}$$

The maximum value, σ_{pc}, of the bridging stress–displacement curve is $2\sigma_0$ and is obtained from Eq. (A.2) by setting $\tilde{\delta}$ into $\tilde{\delta}^*$:

$$\sigma_{pc} = \tau V_f \left(\frac{L_f}{d_f} \right) \tag{A.6}$$

A.2. The fracture energy due to fiber bridging stress

The debonding part of the fracture energy can be estimated by the following equation with σ_B given by Eq. (A.4):

$$G_r = \int_0^{\delta^*} \sigma_B(\delta)\, d\delta = \frac{5}{3}\sigma_0 \delta^* \tag{A.7}$$

The fracture energy due to fiber pull-out can be given by the following equation with σ_B given by Eq. (A.5):

$$G_c = \int_{\delta^*}^{L_f/2} \sigma_B(\delta)\, d\delta = 2\sigma_0 \left\{ \frac{1}{3}\left(\frac{L_f}{2} \right) - \delta^* \right\} \tag{A.8}$$

The fracture energy due to fiber bridging stress can be obtained from Eqs. (A.7) and (A.8):

$$G_b = G_r + G_c = \frac{\sigma_0}{3}(L_f - \delta^*) \approx \frac{1}{6}\tau V_f d_f \left(\frac{L_f}{d_f} \right)^2 \tag{A.9}$$

where δ^* is neglected when $\delta^* \ll L_f$.

References

[1] Aveston J, Kelly A. Theory of multiple fracture of fibrous composites. J Mater Sci 1973;8(3):352–62.
[2] Li VC, Wang Y, Backer S. A micromechanical model of tension softening and bridging toughening of short random fiber reinforced brittle matrix composites. J Mech Phys Solids 1991;39(5):607–25.
[3] Li VC. Postcrack scaling relations for fiber reinforced cementitious composites. J Mater Civil Eng 1992;4(1):41–57.
[4] Li VC, Leung CKY. Steady-state and multiple cracking of random fiber composites. J Eng Mech 1992;118(11):2246–64.
[5] Stang H, Li VC, Krenchel H. Design and structural applications of stress–crack width relations in fibre reinforced concrete. Mater Struct 1995;28:210–9.
[6] Kabele P, Horii H. Analytical model for fracture behaviors of pseudo strain-hardening cementitious composites. J Mater Concr Struct Pavements, JSCE 1996;30(532):209–19.
[7] Li VC, Hashida T. Engineering ductile fracture in brittle–matrix composites. J Mater Sci Lett 1993;12:898–901.
[8] Kanda T, Lin Z, Li VC. Tensile stress–strain modeling of pseudo strain hardening cementitious composites. J Mater Civil Eng 2000;12(2):147–56.
[9] Stang H, Li VC. Extrusion of ECC-material. In: Reinhardt HW, Naaman A, editors. Proceedings of High Performance Fiber Reinforced Cement Composites 3 (HPFRCC3). Chapman & Hall; 1999. p. 203–12.
[10] Mu B, Li ZJ. Tensile failure of short fiber-reinforced composites. Key Eng Mater 1998;145–149:607–12.
[11] Li Z, Mu B, Chang TYP, Hsu C-T. Prediction of overall tension behavior of short fiber-reinforced composites. Int J Solids Struct 1999;36:4071–87.
[12] Shah SP, Shao Y. Extrusion processing of fiber-reinforced cement–matrix composites. ASME MD 1994;52:205–16.
[13] Shao Y, Markunte S, Shah SP. Extruded fiber-reinforced composites. Concr Int 1995;April:48–52.
[14] Akkaya Y, Peled A, Shah SP. Parameters related to fiber and processing in cementitious composites. Mater Struct 2000;33:515–24.
[15] Marshall DB, Cox BN. A *J*-integral method for calculation steady-state matrix cracking stresses in composites. Mech Mater 1988;7:127–33.
[16] Li VC. From micromechanics to structural engineering—The design of cementitious composites for civil engineering applications. JSCE J Struct Mech Earthquake Eng 1993;10(2):37–48.

[17] Li VC, Chan Y-W. Determination of interfacial debond mode for fiber-reinforced cementitious composites. J Eng Mech 1994;120(4):707–19.
[18] Kanda T, Li VC. Interface property and apparent strength of high-strength hydrophilic fiber in cement matrix. J Mater Civil Eng 1998;10(1):5–13.
[19] Easley TC, Faber KT, Shah SP. Use of a crack-bridging single-fiber pullout test to study steel fiber/cementitious matrix composites. J Am Ceram Soc 1999;82(12):3513–20.
[20] Milewski JV. A study of the packing of milled fiberglass and glass beads. Polym-Plast Technol Eng 1974;3(1):101–20.
[21] Evans KE, Gibson AG. Prediction of the maximum packing fraction achievable in randomly oriented short-fibre composites. Compos Sci Technol 1986;25:149–62.
[22] Shao Y, Shah SP. Mechanical properties of PVA fiber reinforced cement composites fabricated by extrusion processing. ACI Mater J 1997;94(6):555–64.
[23] Takashima H, Mayagai K, Hashida T. Fracture properties of discontinuous fiber reinforced cementitious composites manufactured by extrusion molding. Proceedings of JCI International Workshop on Ductile Fiber Reinforced Cementitious Composites 2002, in press.
[24] Wu H-C, Li VC. Trade-off between strength and ductility of random discontinuous fiber reinforced cementitious composites. Cem Concr Compos 1994;16:23–9.